Journal of Electroanalytical Chemistry 856 (2020) 113633

Contents lists available at ScienceDirect

Journal of Electroanalytical Chemistry

journal homepage: www.elsevier.com/locate/jelechem

$Na_{0.4}(Mn_{0.33}Co_{0.33}Ni_{0.33})O_2$ surface grafted with SnO nanorods: A cathode materials for rechargeable sodium ion batteries

J. Richards Joshua [a], Y.S. Lee [b], T. Maiyalagan [c], N. Nallamuthu [d], P. Yuvraj [a], N. Sivakumar [a,*]

[a] PG and Research Department of Physics, Chikkaiah Naicker College, Erode, Tamilnadu, 638004, India
[b] Department of Applied Chemical Engineering, Chonnam National University, Gwangju, South Korea
[c] Electrochemical Energy Laboratory, Department of Chemistry, SRM Institute of Science and Technology, Kattankulathur, 603203, India
[d] Department of Physics, Multifunctional Materials Laboratory, International Research Centre, Kalasilingam Academy of Research and Education, Krishnakoil, Tamilnadu, 626126, India

ARTICLE INFO

Keywords:
NIBs
Sn coated
Surface coating
High capacity

ABSTRACT

Improving rechargeable Na-ion batteries (NIB) with high specific capacity and stability is still a big challenge. In this report, P2-type $Na_{0.4}(Mn_{0.33}Co_{0.33}Ni_{0.33})O_2$ is act as a cathode material for NIBs prepared by hydrothermal method. SnO is coated on the surface of $Na_{0.4}(Mn_{0.33}Co_{0.33}Ni_{0.33})O_2$ layer to enhance its cycling stability. The coating of SnO is not influenced in the morphology of $Na_{0.4}(Mn_{0.33}Co_{0.33}Ni_{0.33})O_2$ which was confirmed by XRD and SEM analysis. HRTEM images illustrates that SnO is successfully wrapped around the surface $Na_{0.4}(Mn_{0.33}Co_{0.33}Ni_{0.33})O_2$ it contributes a effective coating layer between the surface of the electrolyte and the $Na_{0.4}(Mn_{0.33}Co_{0.33}Ni_{0.33})O_2$. The P2-type $Na_{0.4}(Mn_{0.33}Co_{0.33}Ni_{0.33})O_2$ material delivers 141 $mAhg^{-1}$ of reversible capacity in a voltage range of 0–3.5 V. SnO coated P2-type $Na_{0.4}(Mn_{0.33}Co_{0.33}Ni_{0.33})O_2$ material exhibits good capacity of about ~80% after 100 cycles. On SnO coating the surface size of the P2-type $Na_{0.4}(Mn_{0.33}Co_{0.33}Ni_{0.33})O_2$ reduces the electrolyte decomposition and expedite the smooth transportation of Na^+ ions. The surface modification on the P2-type $Na_{0.4}(Mn_{0.33}Co_{0.33}Ni_{0.33})O_2$ by the SnO nanorods is responsible for the enhanced electrochemical performances.

1. Introduction

Na-ion battery (NIB) has currently attained the great interest within the researchers which can be the alternative to LIB for energy storage applications [1–4], because sodium is eco-rich and cost effective as compared to lithium. The great challenge for commercialization of NIBs battery to develop electrode materials with high capacity and good stability. Lithium ion battery dominates the battery world because they give high energy density [5–9]. Alternatively sodium shares its most of the properties with lithium and it has attained great interest in the development NIBs [10–13]. Due to its cost efficient, natural abundance and sustainability at high temperatures, currently NIBs have attracted the researchers attention for the large scale grid-level energy storage applications [14,15]. The commercial anode (graphite) of LIBs cannot be used for NIBs due to its low capacity. In that even, the immense effort has been made for finding the suitable anodes for NIBs. By now several anode review articles has been reported for NIBs [16–19].

In the modernistic years, researchers have put forward a great stretch to prepare cathode materials with high efficiency and stability through various compounds such as layered oxide compounds, polyanion compounds. The layered oxides are considered as a assuring candidates as high capacity cathode materials for NIB. Sodium-based layered materials are categorized into two main groups using the classification which was proposed by Delmas et al. [20]. O3-type or P2 type, in which the sodium ions are accommodated at octahedral or prismatic sites, respectively. Commonly P2 – type materials are more suitable for SIBs on comparing with O3-type materials because of its large interlayer spacing and structural stability [21]. For P2-type materials, the compounds are usually stabilized into $NaMO_2$ (M = Ni, Co, Mn, Fe, Cr) [22–24]. Sodium ion in P2-type structure can diffuse directly between face –sharing trigonal prismatic sites which results in good electrochemical performances on comparing with O3- type structure. But the disadvantage of P2- type oxides over removal of sodium ions at high voltage which is bounded to capacity fading [25]. The Polyanion compounds like $Na_3V_2(PO_4)_3$ [26], $Na_2FeP_2O_7$ [27],$Na_2MnP_2O_7$ [28],$Na_2CoP_2O_7$ [29], $Na_7V_3(P_2O_7)_4$ [30, 31]. On comparing with the P2 type materials the polyanion compounds

* Corresponding author.
E-mail address: nskdnp@gmail.com (N. Sivakumar).

https://doi.org/10.1016/j.jelechem.2019.113633
Received 2 July 2019; Received in revised form 16 October 2019; Accepted 5 November 2019
Available online 11 November 2019

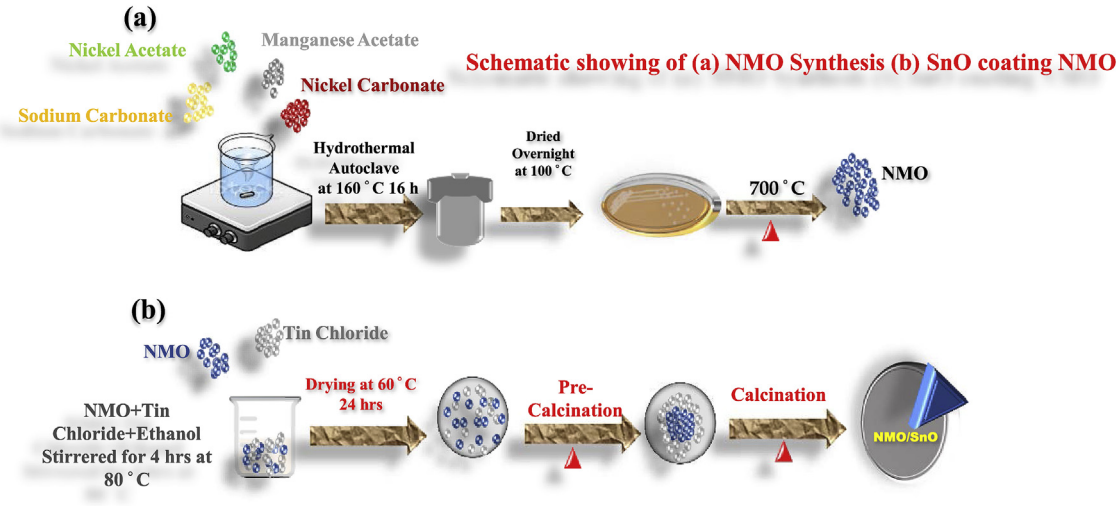

Fig. 1. Schematic showing of (a) NMO synthesis (b) SnO coating NMO.

the capacity and the capacity retention was also less in polyanionic compounds [32]. Types of cathode materials evaluated in NIBs include layered oxides $Na_{1.0}Li_{0.2}Ni_{1/4}Mn_{3/4}O_2$ [33], Na_xCoO_2 [34], $Na_{2/3}(Ni_{1/3}Mn_{2/3})O_2$ [35], $Na(Ni_{1/2}Mn_{1/2})O_2$ [36], $NaCrO_2$ [37,38], Na_xMnO_2 [39–42], Na_xVO_2 [43], $Na_{0.44}MnO_2$ [43–48] and a new type of high capacity, reversible bi-layered sodium $Na_xV_2O_5$ vanadium oxide [49].

Manikandan et al. [50] prepared P2 – type $Na_{0.5}Ni_{0.25}Mn_{0.75}O_2$ through facile sol-gel method, delivers large discharge capacity about 200 $mAhg^{-1}$ 1.5 V and 4.5 V. Kaliappan et al. [51] prepared $Na_{0.67}Ni_{0.13}Co_{0.13}Mn_{0.54}O_2$ reported that the capacity was reduced to 50% at 1C. The results shows that, decreasing the irreversible capacity during cycling plays an significant factor in the evolution of NIBs.Xiao-Hua et al. [52] reported the mechanish via graphene connection of P_2–$Na_{2/3}Ni_{1/3}Mn_{5/9}Al_{1/9}O_2$ as the enhanced electrode materials for NIBs.The connection between formed RGO-NMA shows the capacity of about 138 $mAhg^{-1}$ with good stability and cycling performance. The enhanced performance is due to reduced particle size and apparent Na^+ diffusion.

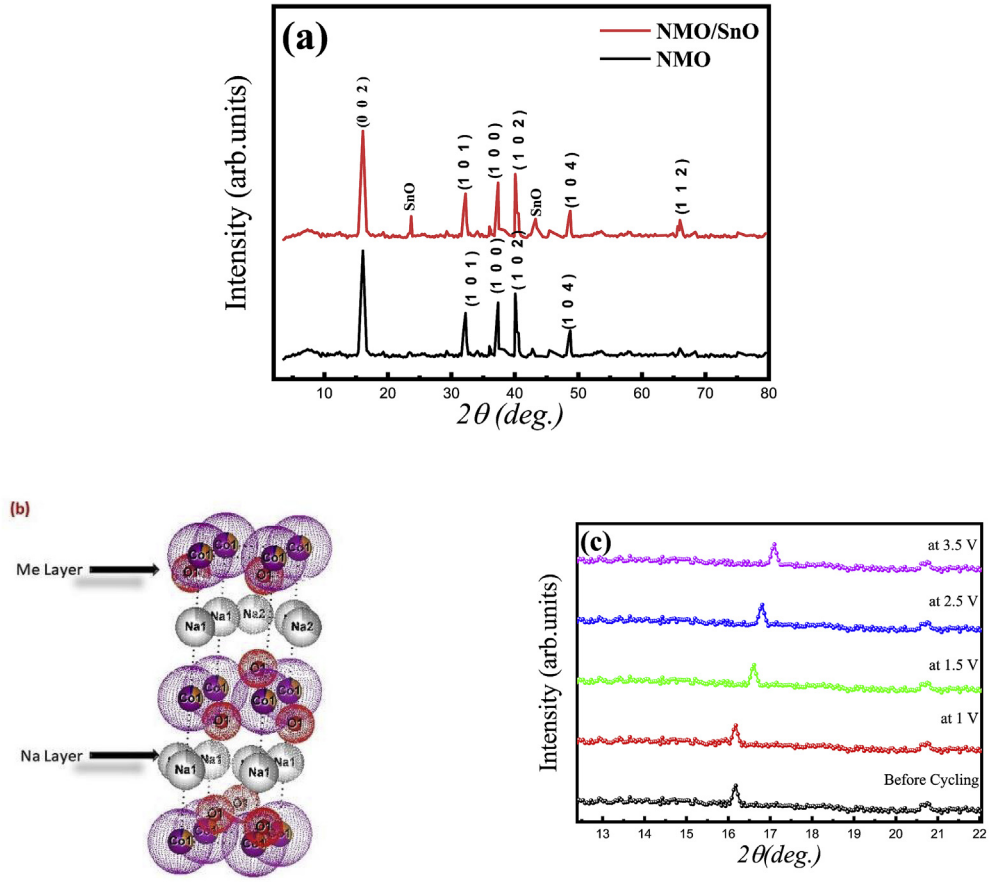

Fig. 2. (a) XRD pattern for NMO and NMO/SnO, (b) Structure of P2 type unit cell, (c) XRD pattern for different cycling voltages.

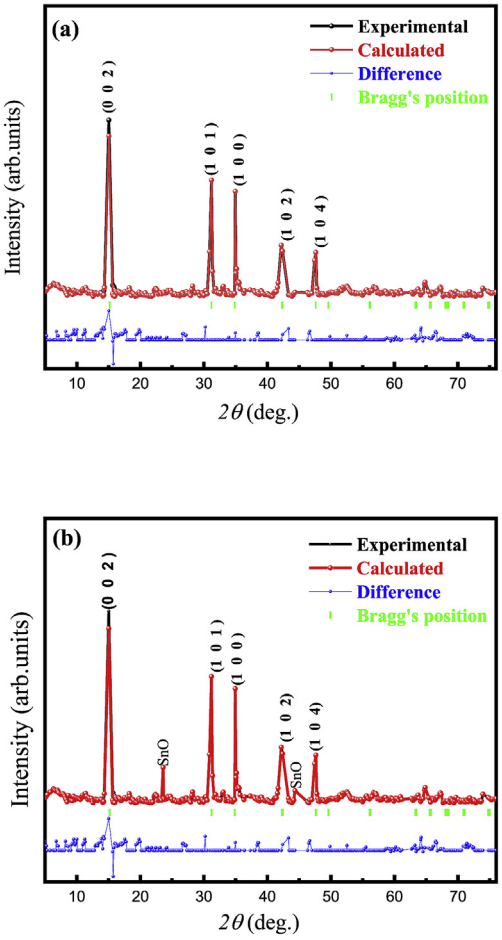

Fig. 3. (a) Rietveld refinement of NMO, Fig. 3(b) NMO/SnO.

Table 1
Results of ICP-AES analysis for NMO and NMO/SnO samples.

	Na	Mn	Ni	Co	Sn
Ratios by ICS analysis					
NMO	0.411	0.37	0.288	0.277	0
NMO/SnO	0.430	0.32	0.294	0.310	0.222
Calculated ratios					
NMO	0.400	0.33	0.33	0.33	0
NMO/SnO	0.400	0.33	0.33	0.33	0.200

Carbon coating helps to enhance the electrical conductivity of cathode materials by reducing the interaction between electrode with the electrolyte. The carbon coated materials has large specific surface area which accomdates with the thickness and decreases the volumetric densities on the surface of the electrodes. Cho et al. [53] have reported nanoscale coating of metal oxides on cathode materials (Al_2O_3, ZrO_2 … etc). Wang et al. [54] founded the modification in the surface of $LiCoO_2$ with MgO coating decreased the electrolyte decomposition and enhanced cyclic perfomance. Kim et al. [55] prepared ZrO_2 coated $LiCoO_2$ cathode materials shows slight capacity loss after 70 cycles. At the same time $LiCoO_2$ gives 60% of its initial capacity after 30 cycles. Recently, $FePO_4$ are considered as a promising coated material used to enhance the electrochemical property of cathode material because it was electrochemically active and low cost material [56–59]. Liu et al. [60] have described the enhanced cycling performance of $FePO_4$ coated $LiNi_{0.5}Mn_{1.5}O_4$ cathode material. Xiao et al. have [61] synthesized $LiNi_{0.5}Mn_{1.5}O_4$ through hydrothermal via carbonate precipitation method and then prepared $FePO_4$ coated $LiNi_{0.5}Mn_{1.5}O_4$ by atomic layer deposition (ALD). Rahul et al. [62] prepared ZnO coated $LiNi_{0.5}Mn_{1.5}O_4$ the capacity retention after 50 cycles for pure and ZnO coated $LiNi_{0.5}Mn_{1.5}O_4$ was about 91 and 97% respectively. Tin oxide is one of the most attracting material which is applicable for several electrochemical storage applications[63]. The large volume expansion of tin oxide during charging and discharging cycles leads pulverization of electrodes and drastic drop in the performance of solid state batteries. It can be averted by decreasing of the size of tin oxide to nano or coating with carbon/metal oxide based nanomaterials. However, the cohesive energy of tin oxide can enhance the agglomeration of particles during electrochemical cycling and it reducing their stability. Hence, it need to disperse nano tin oxide doped with metal oxide supports with strong bonding to prevent the agglomeration of particles and enhance electrochemical stability. Previously ZnO, CuO, MgO, $FePO_4$ was used as the coating materials for the energy storage applications.

This has motivated us to prepare the P2-type $Na(Mn_{0.33}Co_{0.33}Ni_{0.33})O_2$ electrode materials for NIBs and By considering the various advantages of Sn, we choose Sn (TIN) as the coated material. According to our best knowledge and studying various references we are the first to report SnO coated cathode materials for NIB batteries.

1.1. Experimental procedure

The Schematic system for preparation was shown in Fig. 1. P2-type $Na_{0.4}$ $(Mn_{0.33}Co_{0.33}Ni_{0.33})O_2$ was prepared by hydrothermal method. The stochiometry amount of $Na(NO)_3$ (sigma Aldrich), $Co(NO)_3$ (Sigma Aldrich), $Mn(NO)_3$ (sigma Aldrich), $Ni(NO)_3$ (sigma Aldrich) was

Table 3
Refined Crystal sites and atomic occupancies of the NMO sample.

Atom	x	y	z	Biso	Occ
Na1	0.53900	0.1900	0.2500	0.00	0.333
Na2	0.0000	0.667	0.2500	0.00	0.333
Co1	0.0000	0.0000	0.0000	0.00	0.041
Ni1	0.0000	0.0000	0.0000	0.00	0.233
Mn1	0.0000	0.0000	0.0000	0.00	0.690
O	0.3333	0.6667	0.0872	0.00	1.000

Table 4
Refined Crystal sites and atomic occupancies of the NMO sample.

Atom	x	y	z	Biso	Occ
Na1	0.53900	0.1900	0.2500	0.00	0.333
Na2	0.0000	0.667	0.2500	0.00	0.333
Co1	0.0000	0.0000	0.0000	0.00	0.041
Ni1	0.0000	0.0000	0.0000	0.00	0.233
Mn1	0.0000	0.0000	0.0000	0.00	0.690
O	0.3333	0.6667	0.0872	0.00	1.000
Sn	0.000	0.0000	0.0000	0.80	1.000

Table 2
Refined crystal parameters of the prepared samples.

Sample	Phase	Fraction	a(Å)	c(Å)	R_p	wR_p	Gof
$Na_{0.4}(Mn_{0.33}Co_{0.33}Ni_{0.33})O_2$	P2	100%	2.877	11.162	2.79	4.42	1.96
	Sn	0					
$Na_{0.4}(Mn_{0.33}Co_{0.33}Ni_{0.33})O_2$–SnO	P2	91.6%	2.884	11.186	2.38	4.20	1.39
	Sn	8.4%					

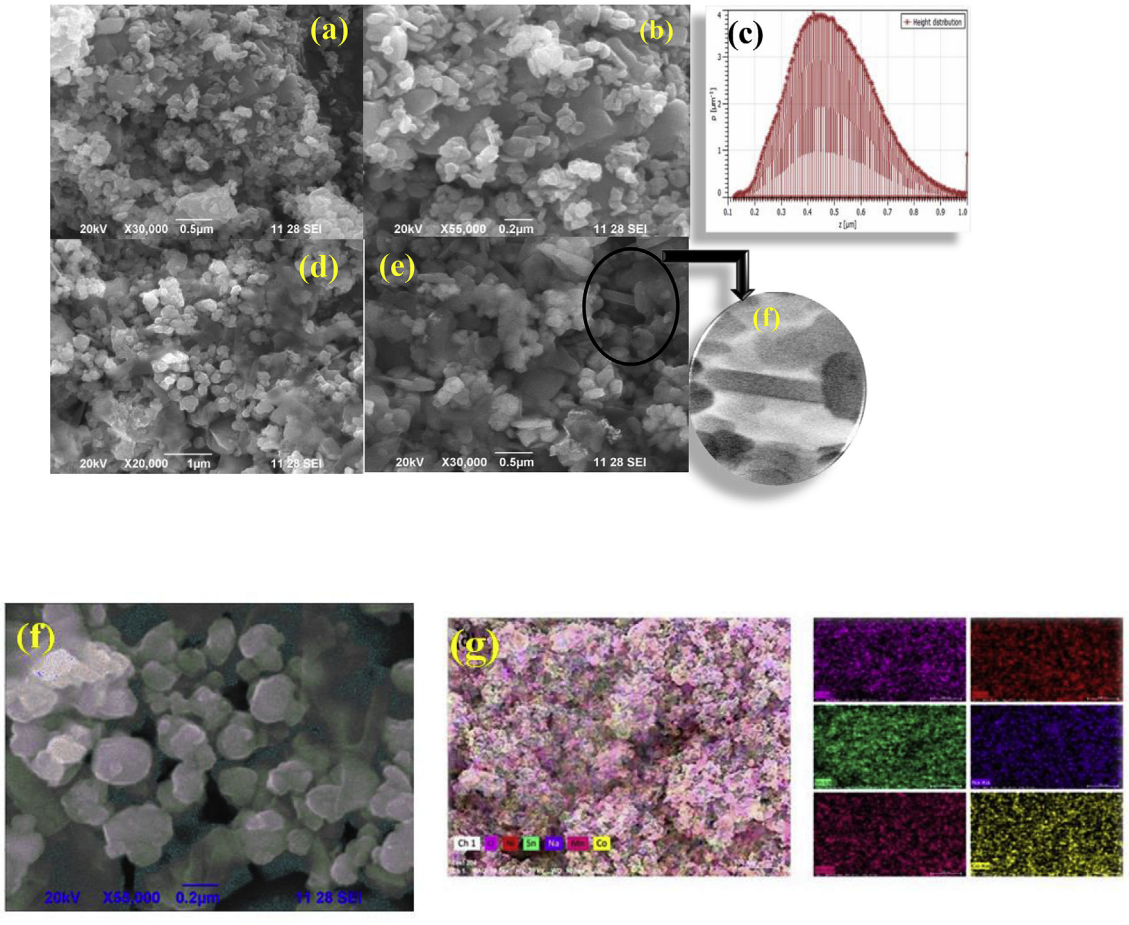

Fig. 4. (a,b) The SEM images of NMO, (c)- the size distribution of the rods formed by coating of Sn, (d,e)- NMO/SnO, (f) – The X-ray inverted image of the rods formed on the NMO surface, (g)- The elemental mapping of the NMO/SnO.

dissolved in 50 ml of de-ionized water and allowed to stirrer for few hours and then prepared solution was transferred into the Teflon lined autoclave and maintained at 160^{O} C for 16 h. Then the sample was washed two to three times with distilled water and ethanol. The sample was dried in the oven at 100 ^{O}C overnight for 10 h and sintered for 700 ^{O}C for 5 h with heating rate of 1 °C min^{-1}.

1.2. Preparation of Sn coated $Na_{0.4}(Mn_{0.33}Co_{0.33}Ni_{0.33})O_2$

For the preparation of SnO coated $Na_{0.4}(Mn_{0.33}Co_{0.33}Ni_{0.33})O_2$, 0.2 mol of $SnCl_2$ was dissolved in 50 ml of ethanol and sonicated for 15 min in an ultra sonicator. Then the sample was allowed to stirrer for 2 h and then prepared $Na_{0.4}$ $(Mn_{0.33}Co_{0.33}Ni_{0.33})O_2$ was slowly added to the above solution and maintained at 60 ^{O}C and The dried samples are made into pellets and undergoes two-step calcination process: first the sample was precalcinated at 300 °C fir 3 h and finally calcined at 550 °C for 6 h.The sample will denoted as P2-type $Na_{0.4}$ $(Mn_{0.33}Co_{0.33}Ni_{0.33})O_2$-NMO and NMO/SnO.

1.3. Materials characterization

The crystal parameters are analysed using X-ray diffraction (XRD,

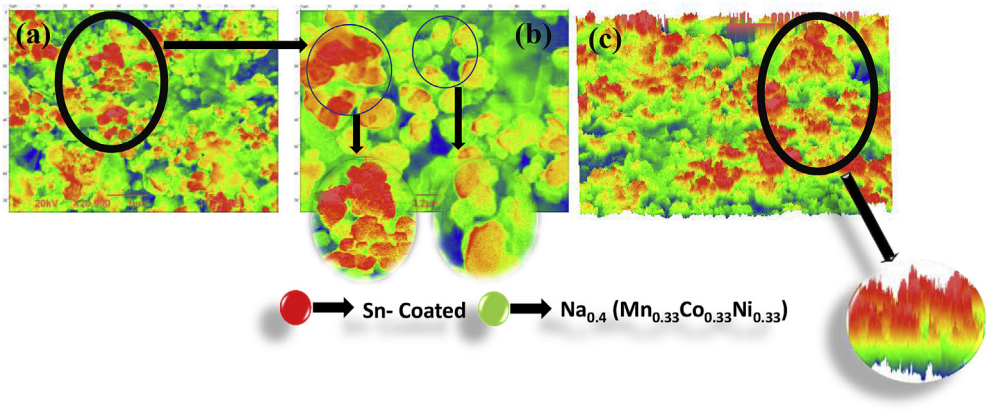

Fig. 5. (a) (b) The SEM images are analysed using Data analysing and processing software, (c) 3 dimensional view of the coated sample.

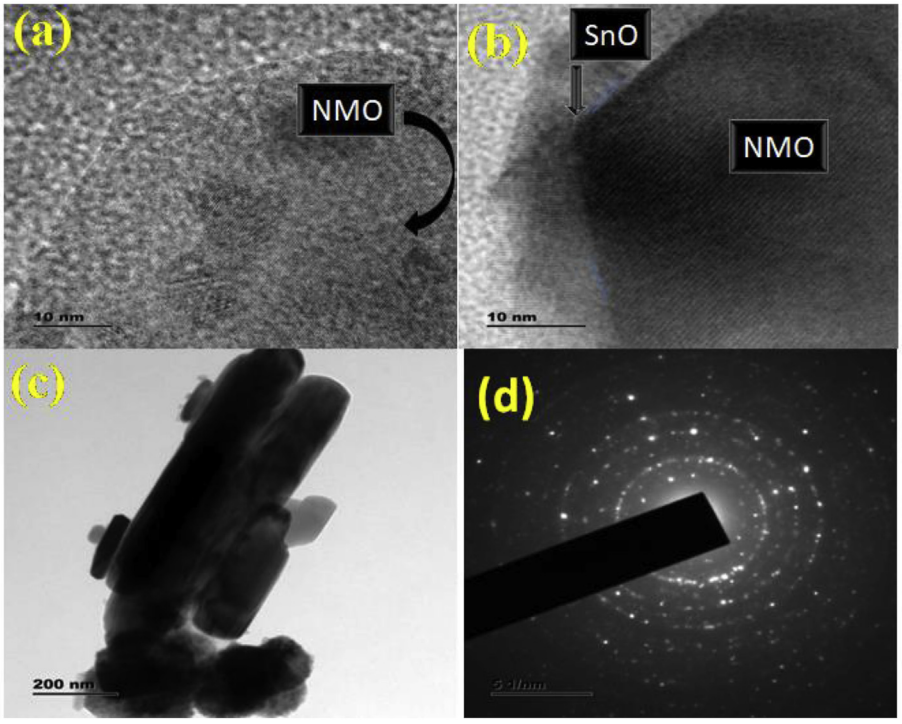

Fig. 6. (a,b)- The HR-TEM images of the NMO and NMO/SnO, (c) – the image of the single rod on the surface of NMO (d)- SAED pattern shows the high crystallinity of NMO/SnO.

SmartLab, Rigaku) with CuKα as the radiation source in the range of 10°–80°. The scanning electron microscope (SEM, ZEIIS SUPRA55) are used in analysing the morphological nature of the samples. To analyse the coating of SnO on the surface of the NMO (HRTEM, FEI TECNAIG2F30) at 300 kV were used to examine the thickness of the coating. The data analysing and processing software to analysis the morphological structure of the prepared material. Land CT2001A battery testing system was used to analyse the electrochemical properties of the prepared samples.

1.4. Electrochemical measurements

The electrochemical properties of NMO and NMO/SnO was analysed by using battery testing system as mentioned above. To assemble the electrodes, the prepared materials are mixed with polyvinylidene (PVDF) as the binder and carbon black (CB) at the ratio of 8:1:1 are grained well using agitate mortar. Then NMP (N- methylpyrrolidone) was added dropwise to make a slurry. The prepared slurry was casted into a aluminium foil and dried in the oven at 120° for 5 h. The loading mass of the active material is about 1–2 mg. For the electrochemical performance sodium was used as an anode and prepared material as cathode. The ratio of (1:1) ED:DMC was mixed with $NaClO_4$ was used as an electrolyte. The cyclic voltametry was measured on a Solartron 1260 + 1287 electrochemical workstation at a voltage range of about 0–3.5 V.

2. Result and discussion

The X-ray diffractions, the correlative Rietveld refinement results of the sample is shown in the Figs. 2a and 3. The diffractions of the sample has well matched with the standard phase group of $P6_3/mmc$ (PDF:00-54-0894) [64,65]. From the two prepared materials NMO/SnO shows high crystalline nature without any impurity secondary phase. However, in Fig. 2, the two peaks at $2\theta = 23°$ and $2\theta = 46°$ stand for SnO. The presence of SnO is due to coating of SnO over the surface of the NMO but it does not influence the nature of the P2-phase. According to the refinement results are shown in the Table 1. The refined parameter has

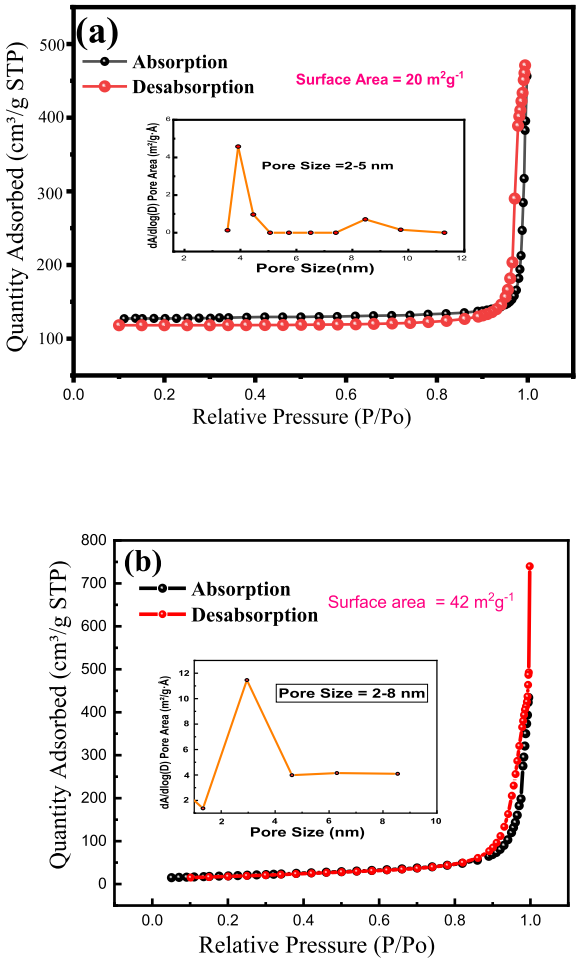

Fig. 7. Nitrogen physisorption isotherms of (a) $Na_{0.4}(Mn_{0.33}Co_{0.33}Ni_{0.33})O_2$; and (b) Sn- Coated $Na_{0.4}(Mn_{0.33}Co_{0.33}Ni_{0.33})O_2$ samples with inset showing BJH pore size distribution.

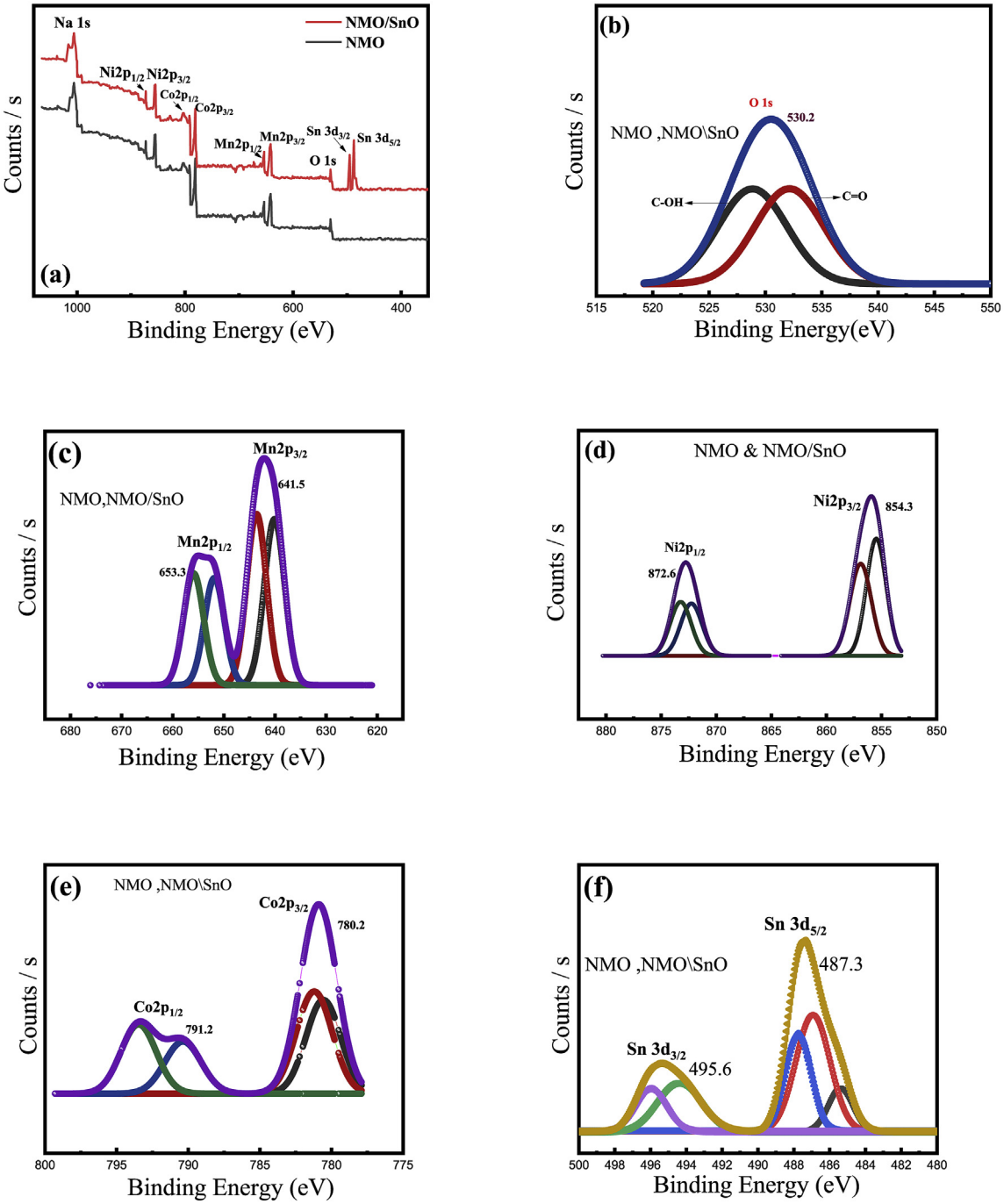

Fig. 8. (a) XPS spectrum of NMO and NMO/SnO (b) O1s (c) Mn 2p (d) Ni 2p (e) Co 2p (f) Sn 3d

slightly increased on coating of Sn on the surface of the NMO.

The stimulated structure of the prepared NMO sample was shows that, the material indexed to P2-phase will be smoothed of Na layers and transition – metal in the oxygen framework and the hexagonal sites in a unit cell was occupied by Na^+ ion shown in Fig. 2b [66]. The obtained parameters and the refinement results are summarized in the Tables (1)–(4). While the parameter C (11.162 Å) of NMO and for NMO/SnO the C parameter has increased slightly (11.186 Å). The lattice parameter increases due to increase ionic radii and which denotes the high crystallinity of the sample after coating with SnO which is confirmed by using ICP analysis shown in Table 1.

The SEM analysis shows the morphological information of the samples. Fig. 4a,b shows the SEM images of the NMO, the size of NMO particles varies from 0.5 to 1 μm, Fig. 4c,d shows the SEM image of SnO coated. In Fig. 4c minute rods has been formed which was inserted in 4e the gray inverted image of the formed rods and Fig. 4c shows the height distribution of the rods on the surface of NMO. The Fig. 4 (f,g) shows the elemental mapping of the prepared NMO and NMO/SnO. Fig. 5 shows the analysis on the surface of the SEM images, to confirm the SnO coating on the surface of the NMO and also to find the inner depth of the coated sample. The Fig. 5b confirms that the SnO was coated on the surface of the NMO and the dark red region at the tip of the rods indicates the presence of the SnO coating. Fig. 5c shows the 3-dimension view of the prepared sample, the 3D view shows the top and bottom intensities of the formed rods. These analysis are carried out by using computed stimulated software for analysing the surface to find the stress and strain of the prepared samples NMO and NMO/SnO. Fig. 6 shows the HRTEM images of the NMO and NMO/SnO samples. The Fig. 6a shows the uncoated

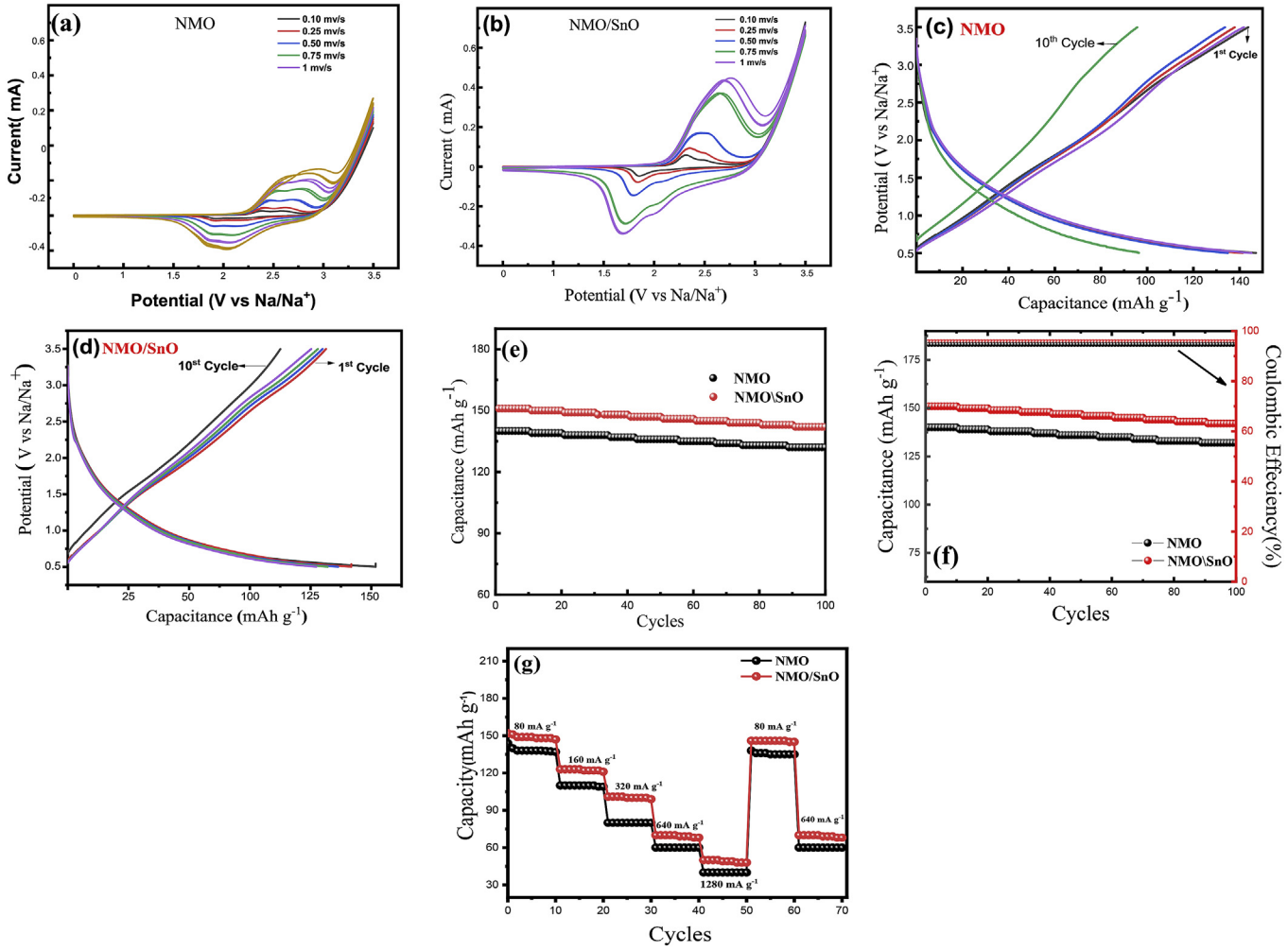

Fig. 9. Cyclic voltammograms of (a) NMO (b) NMO/SnO, (c)Charge/discharge curves of NMO, (d) NMO/SnO, (e) Cycling performance of NMO and NMO/SnO at 80 mAg^{-1}, (f) Rate performance of as-prepared materials in the potential window 1.0–3.5 V for 100 cycles.

NMO sample, the dark region at the centre denotes the presence of NMO and in Fig. 6b the slight a white-black layer was formed around the centre NMO is SnO, for NMO/SnO the particle thickness is less than 10 nm was distributed on the surface of NMO. The Fig. 6b confirms that SnO was coated on the surface of the NMO which matches with the Fig. 5.

The BET analysis has been taken for analysing the surface and for finding the surface volume and pore size distribution of the prepared samples. Fig. 7, the nitrogen physisorption and BJH pore size distribution for all the samples reported here. Both NMO and NMO/SnO shows the defined hysteresis loop which is attributed to a Type-IV isotherm associated with a mesoporous nature. The BET surface area of the NMO is about 20 m^2g^{-1} with a pore distribution between 2 and 5 nm was shown in Fig. 7a. Interestingly, after coating Sn to the surface of the NMO the surface area increase to 40 m^2g^{-1} with a pore size ranges from 2 to 8 nm Fig. 7b. By the encapsulation of SnO the surface of the NMO is expected to acquires a high discharge capacity and improved cycling performance.

To analysis the chemical composition and oxidation states of the NMO samples, XPS analysis was performed. The Fig. 8a compares the spectra of NMO and NMO/SnO samples. The peak around 1040.3, 854.2, 780.22, 641.5, 530.56 confirms the presence of Na, Ni, Co, Mn and O respectively. Fig. 5c shows the deconvoluted spectra of the individual spin orbit. The peak formed around 641.5 and 653.3 eV corresponds to the $Mn2p_{3/2}$ and $Mn2p_{1/2}$ shows the oxidation states of the Mn. Thus the oxidation state of the Mn was confirmed as +4 [67]. The Fig. 8d shows the binding energies formed at 854.3 and 872.6 eV which denotes the oxidation peak of the Ni as $Ni2p_{3/2}$ and $Ni2p_{1/2}$, the oxidation states of the Ni was confirmed as +2. The distinct peaks was observed at 780.2 and 791.2 eV in Fig. 8e confirms the oxidation state of the Co +3. The binding energies formed at 789.3 are the satellite peaks. The two distinct peaks formed at 487.3 and 495.6 eV indicate the presence of SnO, the oxidation state of the SnO was confirmed [68].

Fig. 9 a, b shows the CV graph of NMO and NMO/SnO coated samples prepared by hydrothermal method. The cyclic voltametry are analysed with different scan rates. The CV analysis with different scan rates are useful to analyse the sodium/disodium insertion process. The Fig. 9a represents the CV curve of NMO sample. With the scan rate of 1 mV/s the NMO samples which represent the dominant redox couples, there are three peaks at 2.53 V, 2 V, 1.8 V which is almost concord with the Mn^{3+}/Mn^{4+} and Ni^{2+}/Ni^{4+}(V vs Na/Na^+) redox reaction respectively. The peak at 2.53 V and 2 V are very clear while the peaks at 1.8 V (vs Na/Na^+) is slight weak than the other two peaks. Moreover, the oxidation peak was observed at 1.8 V which is related to the redox couples of 2.53 V and V (vs Na/Na^+). This indicates the electrochemical reactions at 2.53 V and 2 V are irreversible. The tendency of the oxidation peaks increases and simultaneously the reduction peaks decreases with increasing scan rates. On the other hand for SnO coated NMO samples shows the two dominant anodic/cathodic peaks at 2.3 V/2.6 V and 2 V/2.2 V corresponds to the redox reactions of Mn^{4+}/Mn^{3+},Co^{4+}/Co^{3+},Ni^{4+}/Ni^{3+} respectively [69–71]. The decrease of these peaks are observed upon 3.5 V which indicates the enhanced stability and reversibility of Na^+ intercalation/deintercalation process. Addition to this when the scanning potential is between 3 and 3.5 V the sharp increase in current was

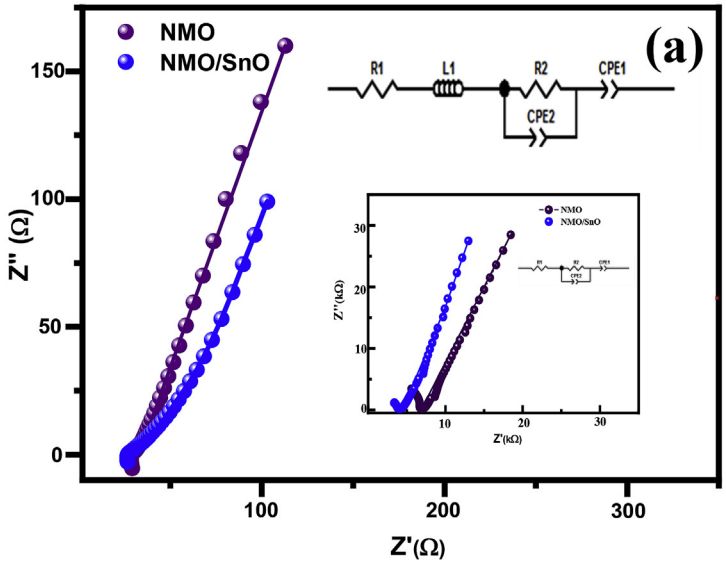

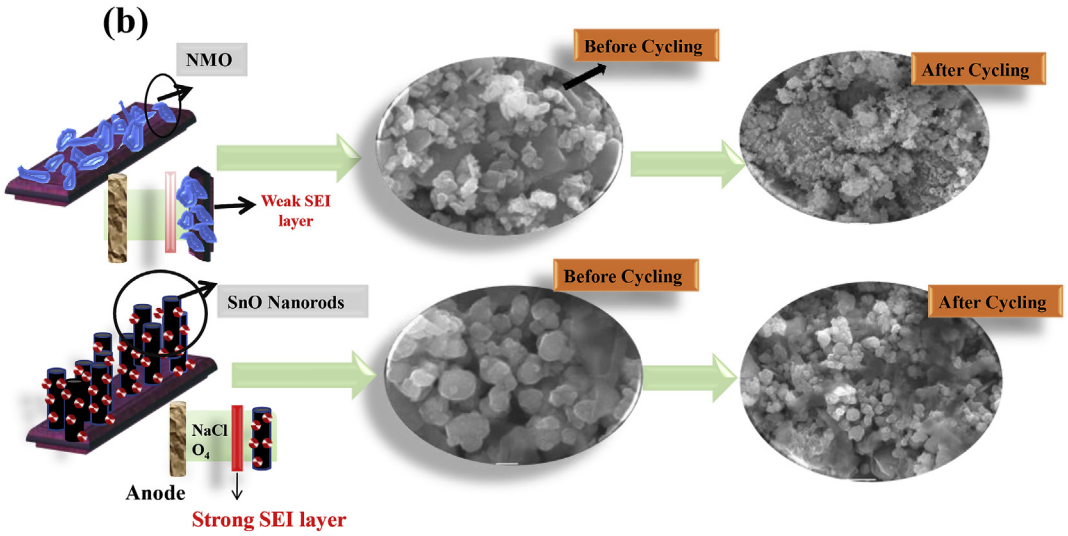

Fig. 10. (a) Nyquist plots of the electrochemical impedance spectra obtained after 100 cycles. Inserted electrochemical impedance spectra before cycling (b) schematic illustration of performance of SnO coating on NMO.

observed which is assigned to the electrolyte decomposition at high voltage range. But SnO coating the electrolyte decomposition was reduced; According to the CV analysis mainly two issues can be noted. (i) The multi reaction of sodium/desodium during charge/discharge process is not accomplished in one step, but two or more steps (ii) in some steps of multireactions of sodium/disodium are reversible, therefore have a little contribution to the discharge capacity in energy storage applications. The results of the cyclic voltametry confirm enhanced performance of NMO/SnO. Fig. 9c,d reports the GCD analysis at 80 mAg^{-1}. In the Fig. 9c the charge-discharge graphs shows two plateaus upon 3.5 V and below 2 V corresponding to the Ni^{2+}/Ni^{4+} and Mn^{3+}/Mn^{4+} redox process respectively, Fig. 9d shows the plateau region between 3 V and 2.5 V which are attributed to the redox process of Ni^{2+}/Ni^{4+},Co^{3+}/Co^{4+} and Mn^{3+}/Mn^{4+}. The observed plateaus are in good accordance with the cyclic voltametry. When charged in higher voltages capacity fade was observed in NMO at 3–3.5 V which is due to phase transistions from P2 – O3 phase which was confirmed by recording xrd pattern at various cycling voltages which is shown in Fig. 1c. The reason for the phase change, at high voltage the cathode materials loses some of the ions into the electrolyte so that the basic P2 phase was changed into O3 phase. The intensity of the P2 was slightly changes from ($2\Theta = 16.08$) at 3–3.5 V. For that confirmation, the XRD patterns are recorded for various voltages like 1 V,1.5 V, 2 V, 3 V, 3.5 V. Till 2.5 V the XRD pattern shows minimal changes in the intensity which is due to cycling but after 3.2 V the phase started to change from P2 to O3($2\Theta = 16.08$ to 17.2). In general, the phase transistions are not only the reason for the capacity fading at higher voltages, the capacity fading is attributed to several phenomena like (i) electrolyte decomposition which is due to electrolyte interface, (ii) Jahn-Teller distortion resulting in Mn^{2+} dissolution into the electrolyte [72], (iii) small internal stress occurs on the surface due to accommodation of larger surface ions of the Na ions [73] and (iv) solvation of ions into the metal oxides [74]. The initial discharge capacity of the

NMO sample is about 141 $mAhg^{-1}$ at 80 mAg^{-1} which is lower than the coated NMO samples. The coated SnO smoothens the plateau above 2.8 V which is also well indicates at cyclic voltametric analysis. The discharge capacity of the NMO/SnO is about 152 $mAhg^{-1}$ at 80 mAg^{-1}. The lower potential of the NMO sample is due to lower surface area of the samples which causes the electrolyte decomposition of ion as mentioned above. By coating with SnO the increase surface area the structural phase transistions from P2–O3 was reduced and smooth transistions over entire voltages.The Fig. 9e shows the long-term cycling perfomance of the NMO and NMO/SnO describes the higher discharge capacity and its capacity fade was observed at prolonged cycling. The capacity retention after 50 Cycles is about 72% the discharge capacity is equal to 102 $mAhg^{-1}$ and for NMO/SnO is about 78% of 118 $mAhg^{-1}$ discharge capacity. The initial discharge fade is due to various phenomena as mentioned above. The discharge capacity drops to 94 $mAhg^{-1}$ after 100 cycles which is lower than NMO/SnO is about 108 $mAhg^{-1}$ after 100 cycles. From the two samples NMO/SnO delivers the discharge capacity of 151 $mAhg^{-1}$ at 80 mAg^{-1} with the capacity retention is about 69%[75].

Rate capability is the important parameter for Sodium-ion batteries. The Fig. 9f shows the rate perfomance of the NMO and NMO/SnO samples. The rate perfomance was analysed between 0 and 3.5 V at different current densities 80 mAg^{-1}, 160 mAg^{-1}, 320 mAg^{-1}, 640 mAg^{-1}, 1280 mAg^{-1} respectively. The NMO samples delivers the capacities of 140, 110, 78, 59, 39 at 80 mAg^{-1}, 160 mAg^{-1}, 320 mAg^{-1}, 640 mAg^{-1}, 1280 mAg^{-1}. Whereas the NMO/SnO samples displayed the capacities of about 151, 123, 101, 72, 48 respectively. If we take 151 $mAhg^{-1}$ at 80 mAg^{-1} as 100%, the capacity retention of the NMO/SnO is about 79% (160 mAg^{-1}),73%(320 mAg^{-1}), 49% (640 mAg^{-1}), 35% (640 mAg^{-1}). The capacitance has been decreased on increasing the current densities. The surface modification using SnO decreases the activation energy for the charge transfer at electrolyte[76,77]. Based on the various results and analysis the SnO coating provides a mechanical support to the cathode material to increase the stability and cycling perfomance.

EIS was used as a major tool to evaluate the kinetic properties. Fig. 10 shows the Nquist plot of NMO and NMO/SnO after cycling and the inserted image are the spectra observed before cycling The NMO plot shows two distinct regions the depressed semi-circle in a medium frequency followed by a quasi straight line in the low frequency region are due to internal resistance and charge transfer resistance (R_{ct}). In NMO/SnO samole the semicircle was reduced, the absence of the semi-circle indicates the negligible role of resistance which is due to diffusion of Na^+ in the SEI layer.

To analyse the influence of SnO coating on the surface, the cycling performance at higher voltages, the Nquist plot of NMO and NMO/SnO was recorded after 100 cycles. The appearance of the depressed semi-circle in the higher region indicates, reduced charge resistance on comparing with the NMO sample. The internal resistance of the NMO sample is about 2.83Ω and charge transfer resistance is about 0.97 Ω. On coating with SnO, the internal resistance was reduced for NMO/SnO is about 2.33 Ω and charge transfer resistance is about 0.33 Ω. This confirms that the influence of the SnO coating increases the electrochemical performances of the materials.The Fig. 10 b shows the illustration and the SEM images of before and after cycling which clearly explains that the SnO protect the cathode materials by forming the strong SEI layer which reduces the contact between the electrode and the electrolyte. So the SnO coating expedite the smooth transport of electrons and enhanced the performance of the cathode materials.

3. Conclusion

Finally SnO coated P2- type layered $Na_{0.4}(Mn_{0.33}Co_{0.33}Ni_{0.33})O_2$ cathode material was successfully prepared. The electrochemical performance of SnO coated NMO delivers capacity of about 118 $mAhg^{-1}$ after 100 cycles with the capacity retention of 80%. The SnO coating on the surface of NMO, increased the surface of the NMO and compressed the decomposition of Na^+ into the electrolyte. The SnO increased the electrochemical performance of the NMO samples. Thus by substituting inactive material and modifying the surface of the cathode material, the cycling and stability of the materials can be improved. The surface modification leads the new way of creating and developing cost effective new cathode materials for NIBs for large scale energy storage applications.

Conflicts of interest

The author declares that there is no conflict of interest regarding the research work reported in this manuscript.

Acknowledgment

The financial assistance from the UGC-SERO (Project No MRP-6836/16) and DST-SERB, New Delhi, India (EMR/2016/006863) were acknowledged.

References

[1] M.H. Han, E. Gonzalo, G. Singh, T. Rojo, Energy Environ. Sci. 8 (2015) 81–102.
[2] N. Ortiz-Vitoriano, N.E. Drewett, E. Gonzalo, T. Rojo, Energy Environ. Sci. 10 (2017) 1051–1074.
[3] Y. Nanba, T. Iwao, B.M. de Boisse, W. Zhao, E. Hosono, D. Asakura, H. Niwa, H. Kiuchi, J. Miyawaki, Y. Harada, M. Okuba, A. Yamada, Chem. Mater. 28 (2016) 1058–1065.
[4] M.-S. Balogun, Y. Luo, W. Qiu, P. Liu, Y. Tong, Carbon 98 (2016) 162–178.
[5] A. Manthiram, J.C. Knight, S. Myung, S. Oh, Y. Sun, Adv. Energy Mater. 6 (2016) 1501010–1501032.
[6] Z. Wei, Y. Gao, L. Wang, C. Zhang, X. Bian, Q. Fu, C. Wang, Y. Wei, F. Du, G. Chen, Chemistry 22 (2016) 11610–11616.
[7] Y. Xie, M. Saubanere, M.L. Doublet, Energy Environ. Sci. 10 (2017) 266–274.
[8] P.K. Nayak, J. Grinblat, M. Levi, O. Haik, E. Levi, S. Kim, J.W. Choi, D. Aurbach, Chemelectrochem 2 (2016) 1957–1965.
[9] M. Sathiya, K. Ramesha, G. Rousse, D. Foix, D. Gonbeau, A.S. Prakash, M.L. Doublet, K. Hemalatha, J.M. Tarascon, Chem. Mater. 25 (2013) 1121–1131.
[10] P.F. Wang, Y. You, Y.X. Yin, Y.G. Guo, J. Mater. Chem. A 4 (2016) 17660–17664.
[11] V. Palomares, P. Serras, I. Villaluenga, K.B. Hueso, J. Carreterogonzalez, T. Rojo, Energy Environ. Sci. 5 (2012) 5884–5901.
[12] X. Xiang, K. Zhang, J. Chen, Adv. Mater. 27 (2015) 5343–5364. Environ. Sci. 5 (2012) 5884-5901.
[13] D. Kim, S.-H. Kang, M. Slater, S. Rood, J.T. Vaughey, N. Karan, M. Balasubramanium, C.S. Johnson, Advanced Energy Materials 1 (2011) 333.
[14] V. Palomares, P. Serras, I. Villaluenga, K.B. Hueso, J. CarreteroGonzalez, T. Rojo, Energy Environ. Sci. 5 (2012) 5884–5901.
[15] H. Pan, Y.S. Hu, Chen, Energy Environ. Sci. 6 (2013) 2338–2360.
[16] B. Jache, Angew Adelhelm, Chem., Int. Ed. 53 (2014) 10169–10173.
[17] M. Dahbi, N. Yabuuchi, K. Kubota, K. Tokiwa, S. Komaba, Phys. Chem. Chem. Phys. 16 (2014) 15007–15028.
[18] Y. Kim, K.H. Ha, S.M. Oh, K.T. Lee, Chem. –Eur. J. 20 (2014) 11980–11992.
[19] C. Bommier, X.L. Ji, Isr. J. Chem. 55 (2015) 486–507.
[20] C. Delmas, C. Fouassier, P. Hagenmuller, Phys. B+C 99 (1980) 81–85.
[21] S. Guo, P. Liu, H. Yu, Y. Zhu, M. Chen, M. Ishida, H. Zhou, Angew. Chem. Int. Ed. 54 (2015) 5894–5899.
[22] Kezhu Jiang, Xueping Zhang, Haoyu Li, Xiaoyu Zhang, Ping He, Shaohua Guo, Haoshen Zhou, ACS Appl. Mater. Interfaces 11 (2019) 14848–14853.
[23] Yongqing Wang, Fengyue Zhao, Yumin Qian, Hongbing Ji, ACS Appl. Mater. Interfaces 10 (2018) 42380–42386.
[24] Ying Bai, Lixiang Zhao, Chuan Wu, Hui Li, Feng Wu, ACS Appl. Mater. Interfaces 8 (2016) 2857–2865.
[25] Y. Fang, L. Xiao, X. Ai, Y. Cao, H. Yang, Adv. Mater. 27 (2015) 5895.
[26] H. Kim, R.A. Shakoor, C. Park, S.Y. Lim, J.-S. Kim, Y.N. Jo, W. Cho, K. Miyasaka, R. Kahraman, Y. Jung, J.W. Choi, Adv. Funct. Mater. 23 (2013) 1147.
[27] C.S. Park, H. Kim, R.A. Shakoor, E. Yang, S.Y. Lim, R. Kahraman, Y. Jung, J.W. Cho, J. Am. Chem. Soc. 135 (2013) 2787.
[28] H. Kim, C.S. Park, J.W. Choi, Y. Jung, Angew. Chem. 55 (2016) 6662.
[29] C. Deng, S. Zhang, B. Zhao, Energy Storage Mater 4 (2016) 71.
[30] Q. Li, B. Lin, S. Zhang, C. Deng, J. Mater. Chem. A 4 (2016) 5719.
[31] Ni Qiao, Ying Bai, Feng Wu, Chuan Wu, Adv. Sci. (2017) 1600275.
[32] Karthikeyan Kaliyappan, Jian Liu, Biwei Xiao, Andrew Lushington, Ruying Li, Tsun-Kong Sham, Xueliang Sun, Adv. Funct. Mater. (1–8) (2017) 1701870.
[33] S. Guo, P. Liu, H. Yu, Y. Zhu, M. Chen, M. Ishida, H. Zhou, Angew Chem. Int. Ed. Engl. 54 (2015) 5894–5899.
[34] R. Berthelot, D. Carlier, C. Delmas, Nat. Mater. 10 (2011) 74.
[35] Z.H. Lu, J.R. Dahn, J. Electrochem. Soc. 148 (2001) A1225.
[36] S. Komaba, T. Nakayama, A. Ogata, T. Shimizu, C. Takei, S. Takada, A. Hokura, I. Nakai, ECS Transactions 16 (2008) 43.
[37] S. Komaba, C. Takei, T. Nakayama, A. Ogata, N. Yabuuchi, Electrochem. Commun. 12 (2010) 355.

[38] X. Xia, J.R. Dahn, Electrochem. Solid State Lett. 15 (2012) A1.
[39] A. Mendiboure, C. Delmas, p. Hagenmuller, J. Solid State Chem. 57 (1985) 323.
[40] R. Stoyanova, D. Carlier, M. Sendova-Vassileva, M. Yoncheva, E. Zhecheva, D. Nihtianova, C. Delmas, J. Solid State Chem. 183 (2010) 1372.
[41] O. Szajwaj, E. Gaudin, F. Weill, J. Darriet, C. Delmas, Inorg. Chem. 48 (2009) 9147.
[42] X. Ma, H. Chen, G. Ceder, J. Electrochem. Soc. 158 (2011). A 1307.
[43] D. Hamani, M. Ati, J.-M. Tarascon, P. Rozier, Electrochemical Communications 13 (2011) 938.
[44] M.M. Doeff, M.Y. Peng, Y. Ma, L.C. De Jonghe, J. Electrochem. Soc. 141 (1994) L145.
[45] C. Didier, M. Guignard, C. Denage, O. Szajwaj, S.I. Saadoune, J. Delmas, Electrochem. Solid State Lett. 14 (2011) A75.
[46] F. Sauvage, L. Laffont, J.M. Tarascon, E. Baudrin, Inorg. Chem. 46 (2007) 3289.
[47] Y.L. Cao, L.F. Xiao, W. Wang, D.W. Choi, Z.M. Nie, J.G. Yu, L.F. Saraf, Z.G. Yang, J. Liu, Adv. Mater. 23 (2011) 3155.
[48] S. Tepavcevic, H. Xiong, V.R. Stamenkovic, X. Zuo, M. Balasubramanian, V.B., C.S. Prakapenka, Johnson, T. Rajh, ACS Nano 6 (2012) 530.
[49] C. Lin, Y. Zhang, L. Chen, Y. Lei, J. Ou, Y. Guo, H. Yuan, D. Xiao, J. Power Sources 280 (2015) 263–271.
[50] P. Manikandan, D. Ramasubramonia, M.M. Shaijumon, Electrochim. Acta 206 (2016) 199–206.
[51] K. Kaliyappan, J. Liu, A. Lushington, R. Li, X. Sun, CnemSusChem 8 (2015) 2537–2543.
[52] Xio-Hua Zhang, Wei-Lin Pang, Fang Wan, Jin-Zhi Guo, Hong-Yan Lu, Jin-Yue Li, Yue- Ming Xing, Jing-Ping Zhang, Xing-Long Wu, ACS Appl. Mater. Interfaces 8 (2016) 20650–20659.
[53] J. Cho, Y.J. Kim, B. Park, Chem.Mater. 12 (2000) 3788.
[54] Y.J. Kim, J. Cho, T.J. Kim, B. Park, J. Electrochem. Soc. 150 (2) (2003). A 1723.
[55] Z. Wang, X. Huang, L. Chen, J. Electrochem. Soc. 150 (2) (2003). A 199.
[56] F.X. Wang, S.Y. Xiao, M.X. Li, et al., J Power Soures 287 (2015) 416–421.
[57] X.Z. Liu, H.Q. Li, E. Yoo, et al., Electrochim. Acta 83 (2012) 253–258.
[58] H.L. Zhang, T.F. song, Electrochim. Acta 114 (2013) 116–124.
[59] A. Manthiram, J.C. Knight, S. Myung, S. Oh, Y. Sun, Adv. Energy Mater. 6 (2016) 1501010–1501032.
[60] D.L. Liu, Y. Bai, S. Zhao, et al., Power Sources 219 (2012) 33–38.
[61] B. Xiao, J. Liu, Q. Sun, et al., Adv. Sci. 2 (2015) 1500022.
[62] Maharaj Raghul, S. Tomar, G. Juan, S. Bures Ram, Katiyar Journal of Power Soures 183 (2008) 334–338.
[63] B.P. Vinayan, S. Ramaprabhu, J. Mater. Chem. A 1 (2013) 3865–3871.
[64] Y.E. Zhu, X. Qi, X. Chen, X. Zhou, X. Zhang, J. Wei, Y. Hu, Z. Zhou, J. Mater. Chem. A 4 (2016) 11103–11109.
[65] Y. Liu, X. Fang, A. Zhang, C. Shen, Q. Liu, H.A. Enaya, C. Zhou, Nanometer. Energy 27 (2016) 27–34.
[66] L.G. Chagas, D. Buchholz, C. Vaalma, L. Wu, S. Passerini, J. Mater. Chem. A 2 (2014) 20263–20270.
[67] J. Hernandez, P. Wrschka, G.S. Oehrlein, J. Electrochem. Soc. 148 (2001) G389.
[68] K. Wang, Z.G. Wu, T. Zhang, Y.P. Deng, J.T. Li, X.D. Guo, Xuo, B.B. Xu, B.H. Zhong, Electrochim. Acta 216 (2016) 51–57.
[69] I. Hasa, D. Buchholz, S. Passerini, B. Scrosati, J. Hassoun, Adv. Energy Mater. 4 (2015) 1400083–1400089.
[70] K. Karthikeyan, S. Amaresh, G.W. Lee, V. Aravindan, H. Kim, K.S. Kang, W.S. Kim, Y.S. Lee, Electrochim. Acta 68 (2012) 246–253.
[71] Ying Bai, Chuan Wu, Feng Wu, Li-xin Yang, Bo-rong Wu, Electrochem. Commun. 11 (2009) 145–148.
[72] Y. Wen, B. Wang, G. Zeng, K. Nogita, D. Ye, L. Wang, Chem. Asian J. 10 (2015) 661–666.
[73] Z. Jian, W. Han, X. Lu, H. Yang, Y.S. Hu, J. Zhou, Z. Zhou, J. Li, W. Chen, D. Chen, L. Chen, Adv. Energy Mater. 3 (2013) 156–160.
[74] S. Komaba, N. Yabuuchi, T. Nakayama, A. Ogata, T. Ishikawa, L. Nakai, Inorg. Chem. 51 (2012) 6211–6220.
[75] D. Buchholz, L.G. Chagas, M. winter, S. Passerini, Electrochim. Adv 110 (2013) 208–213.
[76] Y.S. Meng, D.H. Lee, J. Xu, Physiol. Chem. Phys. 15 (2013) 3304–3312.
[77] Karthikeyan Kaliyappan, Jian Liu, Biwei Xiao, Andrew Lushnigton, Ruying Li, Tsun-Kong Sham, Xueliang Sun, Adv. Funct. Mater. (2017) 1701870.